Mesoporous Anatase TiO_2 Films: Use of Ti K XANES for the Quantification of the Nanocrystalline Character and Substrate Effects in the Photocatalysis Behavior

Paula C. Angelomé,[†] Leandro Andrini,[‡] Mauricio E. Calvo,[§] Félix Gregorio Requejo,*[,‡,☆] Sara A. Bilmes,*[,§,||,☆] and Galo J. A. A. Soler-Illia*[,†,§,☆]

Unidad de Actividad Química, Comisión Nacional de Energía Atómica, UAQ-CAC-CNEA, Avenida Gral Paz 1499, B1650KNA, San Martín, Buenos Aires, Argentina, Departamento Física, FCE, UNLP e INIFTA-IFLP (CONICET), La Plata, Argentina, DQIAyQF, Universidad de Buenos Aires, Pabellón II, Ciudad Universitaria, C1428EHA, Buenos Aires, Argentina, INQUIMAE, Universidad de Buenos Aires, Pabellón II, Ciudad Universitaria, C1428EHA, Buenos Aires, Argentina, and CONICET Avda. Rivadavia 1917, C1033AAJ Buenos Aires, Argentina

Received: December 29, 2006; In Final Form: April 17, 2007

Mesoporous titania thin films with accessible porosity and anatase structure were synthesized on conductive glass or silicon substrates. Ti K-edge XANES was used to assess Ti local coordination. Analysis of the pre-edge region permitted accurate quantification of the degree of crystalline nature of the inorganic walls upon thermal treatment. The substrate has a marked effect: film crystallization takes places at temperatures 100 °C lower in the crystalline Si, with respect to conductive glass. Accordingly, remarkable photocatalytic properties are found in well-crystallized mesoporous titania deposited onto conductive silicon.

Introduction

In the past decade, there has been a manifest interest in nanocrystalline titania thin films. The photoelectronic properties of nanoanatase are interesting for environmental or clean energy applications, such as photovoltaics and photocatalysis. Crystalline structure and particle size are responsible for an efficient light−semiconductor interaction.[1] In addition, there is a quest for high-surface-area coatings that can maximize the interactions between the oxide phase and the pollutants (in photocatalysis) or the electrolytes (in photovoltaics). High-surface-area porous coatings derived from colloidal titania have been explored. However, the pore distributions of these materials are difficult to reproduce, are prone to be widely dispersed, and tend to be blocked by regular-size molecules, such as usual organic pollutants. The mechanical stability of these textural pore systems is also an issue. Surfactant-templated mesoporous thin films are indeed an interesting choice, because of the possibility of reproducibly creating high-surface-area electrodes with continuous robust walls, and regular and accessible pore systems.[2−4] Indeed, mesoporous thin films with well-defined organized pore arrays constitute a unique chance to build a "nanofacility", where controlled processes can be carried out in utterly controlled cavities, which can be tailored at will in terms of wall nature, cavity size, surface, and molecular modifications. Tailoring of these features is a desired goal in catalysis and photocatalysis applications.[5]

The possibility to synthesize mesoporous nanocrystalline titania thin films[6−9] has triggered in the past 3 years a growing number of works dedicated to the optimization of conditions leading to the production of functional titania thin films with efficient photocatalytic or photovoltaic performances.[10−15] Two global strategies have been so far reported in order to obtain nanocrystalline walls: (a) thermal treatment to temperatures higher than the amorphous → anatase transition (in the vicinity of 350−400 °C); (b) use of preformed nanocrystalline particles as building blocks of the inorganic walls. The latter method relies critically on the reproducible synthesis of nanoanatase colloids.[13,16] A critical point of the first path is the control of the nucleation and growth processes taking place within the inorganic walls upon thermal treatment and consequent crystallization. When crystal size exceeds wall thickness, the continuous mesoporous structure usually collapses, leading to a fragile packing of nanocrystallites. The simplest strategy to control this issue is to perform a slow thermal treatment up to temperatures below or near the amorphous to anatase transition, which results in controlled crystallization.[8a,9] The "delayed rapid crystallization" route relies in a short "flash" treatment at 500−700 °C. This method favors a nucleation burst of nanoanatase, followed by a short growth period, resulting in smaller crystallite size.[8b] While a good control of the film crystalline character can be achieved, the kinetics of this process is very sensitive to several external factors, particularly temperature gradients and heat transfer, which makes it difficult to control. Alternatively, a carbonaceous coating can be created within the pores, to avoid the collapse of the mesostructure.[12] This procedure adds, however, further steps to the synthesis procedure.

Previous works rely on X-ray diffraction (XRD) to follow the crystallization process, either discontinuously or in situ.[11,17,18] While XRD is a powerful tool to detect the presence of nanocrystals and estimate crystallite size, its very nature (detection of local crystallization events) is not appropriate to give an accurate view of the behavior of the metal centers throughout the sample. Therefore, spectroscopic tools are needed in order to have a broad picture of the crystallization process, related to the change in the environments of the metal centers, and to gain in quantitative character. Raman spectroscopy has been used to evaluate titania crystal structure and crystallite size;

* Corresponding author. E-mail: requejo@fisica.unlp.edu.ar (F.G.R.); sarabil@qi.fcen.uba.ar (S.A.B.); gsoler@cnea.gov.ar (G.J.A.A.S.-I.).
[†] UAQ-CAC-CNEA.
[‡] DF, FCE, UNLP, and INIFTA, CONICET.
[§] DQIAyQF, Universidad de Buenos Aires.
[||] INQUIMAE, Universidad de Buenos Aires.
[☆] CONICET Buenos Aires.

10.1021/jp069020z CCC: $37.00
Published on Web 06/28/2007

however, there are limitations in the assessment of the extent of crystallization.[19,20] Due to its sensitivity to local symmetries around a specific absorbent atom, X-ray absorption near-edge spectroscopy (XANES) can fill this gap, by affording a quantitative description of the different Ti(IV) environments present in the different crystalline phases or even in amorphous phases.

In anatase the Ti atoms are six-coordinated to oxygen to form a distorted octahedron in such a way that the Ti site symmetry group is D_{2d}. Thus, the pre-edge Ti K XANES structure arises from a 1s to 3d dipole symmetry allowed transition. The final excited states are described by a mixing of 4p and 3d orbitals from Ti central atom and Ti higher shells, respectively.[21−25] This orbital mixing takes place only in noncentrosymmetric environments, as in oxygen-defective Ti environments, Ti atoms in nonregular or amorphous environments, etc. As the degree of mixing depends on Ti−Ti distances, the pre-edge peak intensities are affected by the particular medium-range structure of the sample. Although the precise origin of the individual contributions to this pre-edge structure for titanium oxides is still under discussion,[21,24,25] empirical analyses have been extensively used to gain information related to the coordination geometry of Ti, cationic valence, and medium-range type ordering of the Ti-containing oxides.[23,26,27] These analyses are based on the existing correlation between the normalized height and energy peak positions with the coordination number of Ti.[23] Indeed, it has been established that the intensity of the pre-peaks increases as the central Ti atom site becomes more noncentrosymmetric due to the increase of the degree of orbital p−d mixing. A slightly different approach for a quantitave analysis determining the different contributions from regular or nonregular octahedral Ti environments can be successfully exploited:[31,32] we deconvolute the relative intensities of the individual electronic transitions giving rise to the pre-edge features, as determined by Grunes[25] as an improved method for assessing Ti coordination, especially for distorted environments prevalent specifically in amorphous systems. This procedure is described in detail in the Experimental Section.

Because of this unique local sensitivity for chemically selective studies in particular on Ti oxide based compounds, their structure, and electronics in nanostructured materials, XANES permits assessment of the role of different factors, such as type of substrate, thickness, etc., on both structural and electronics characteristics of Ti sites in TiO_2 films. In this work, we show how XANES can be advantageously used to gather information on the amorphous−anatase transition in mesoporous titania films. Such an accurate assessment of these effects in the crystalline nature of the titania framework is central in the design of efficient high-surface-area photocatalytic systems, which are useful for depollution processes.

Experimental Section

Mesoporous titania thin films were prepared under controlled deposition conditions (withdrawal speed, *T*, relative humidity (RH)), as previously reported.[9] Initial solutions were prepared by mixing $TiCl_4$ in ethanol. Nonionic triblock copolymer Pluronic F127 $[(EO)_{106}(PO)_{70}(EO)_{106}]$ and Brij 58 $[(EO)_{20}C_{16}H_{33}]$ were used as structure-directing agents; the same mass of template (0.675 g) was added to every 0.01 mol of Ti(IV). Water was added under stirring. The final molar ratio in solution was $Ti:H_2O:EtOH = 1:10:40$. Clean conductive indium tin oxide (ITO, Delta Technologies), fluoride-doped tin oxide (FTO), and low-resistivity silicon wafers (n-type doped Si:As, $\rho = 5 \times 10^{-3}$ Ω cm, Crysteco) were used as substrates. Films were produced by dip coating at 2 mm s^{-1} withdrawing speed, under controlled humidity conditions (RH 40−50%). As-prepared films were submitted to successive 24-h treatments at 50% RH and 60, 135, and 200 °C to improve phase separation of the template and cross-linking of the inorganic network.[9,28] Thermal treatment of these stabilized coatings up to temperatures of 300−500 °C was carried out in tubular ovens under still air, using 1 °C min^{-1} temperature ramps; samples were kept at these temperatures for 2 h. Under these conditions, reproducibility and accessibility of the cubic pore systems are ensured.[29]

Mesostructures were characterized by two-dimensional (2D) small-angle X-ray scattering (SAXS) at the D11A-SAXS line at the Laboratório Nacional de Luz Síncrotron (LNLS), Campinas, SP, Brazil, using $\lambda = 1.608$ Å and a sample−detector distance of 650 mm; image plates were used as detectors. Measurements were performed at normal and 3° incidence, in order to determine the mesostructure type and orientation.

The X-ray absorption spectra were measured at the XAS beamline of the LNLS. XANES spectra at the Ti K-edge (4966 eV) were recorded in air at room temperature in fluorescence mode. The intensity I_0 of the incident photon beam was determined by an ionization chamber mounted before the sample, and the fluorescence intensity I_f from the sample was measured averaging the signal from 16 solid-state detectors. The spectra of the samples were expressed as I_f/I_0. All spectra were calibrated using a Ti metallic foil obtained by measuring the intensities I_0 and I_1 from the ionization chambers placed before and after the reference sample. The first point of inflection was used to determine the energy edge absorption position. A Si(111) single crystal was used as monochromator and the vertical aperture of entrance slits was fixed at 0.5 mm to obtain the desired energy resolution of about 1 eV at the Ti K-edge energy value.

X-ray absorption data were analyzed using standard procedures:[30] a linear background was fit to the pre-edge region and then subtracted from the entire spectrum, and the jump of the spectrum was normalized to unity with the post-edge asymptotic value. XANES fits using Gaussian curves for the pre-peaks (A1, A2, A3, and B) plus an extra peak that accounts for the edge rising are shown in Figure 3. All spectra were fitted in the pre-edge region (4960−4980 eV) as in previous studies,[32] using WinXAS[33] to obtain the relative intensity contribution from each fitted Gaussian in each spectrum. Particularly, we use the energy positions of transitions A2 and A3 and their combined area relative to that of all pre-edge features as a measure of Ti 3d occupancy. As in the case of the overall pre-edge feature intensity and location, these relative peak areas can be related empirically to Ti coordination numbers (see Characterization of Local Titania Structure by XANES under Results and Discussion).

Wide-angle X-ray diffraction (WAXRD) patterns were obtained with a Siemens D5000 apparatus (INQUIMAE, UBA), by performing a low-angle-incidence θ-scan on the fixed film sample; the incidence angle was optimized in order to minimize the substrate signal. Scherrer analysis to estimate the crystallite size evolution was carried out on the (101) anatase peak, at $2\theta = 25.4°$. TEM images were collected using a Philips EM 301 transmission electron microscope (CMA, Universidad de Buenos Aires, Argentina) operated at 65 kV. Samples were obtained by scratching the films from the substrate and depositing them on carbon-coated copper grids. Field-emission scanning electron microscopy (SEM) and variable-angle ellipsometry were used to assess film thickness. The reported synthesis conditions for

standard thin films lead to a film thickness of 150 nm after heating treatments.

The photodegradation of salicylate (a model pollutant) was selected because of the reproducibility and availability of comparative data.[34,35] Experiments were performed under bias, in a 3.2 mL three-electrode electrochemical cell using a homemade potentiostat. The setup design and procedure were extensively described in previous work.[34,36] Each experiment started recording a control voltammogram of the TiO_2 film in the dark (0.1 mol dm^{-3} $NaClO_4$, pH 3, N_2 saturated), after which the electrode was polarized at +0.60 V (vs saturated calomel electrode). The system was subsequently illuminated for 90 s, the photocurrent intensity was registered and the optics were adjusted to get maximum photocurrent output. A voltammogram under illumination was then recorded between −0.55 and 0.9 V, at 50 mV/s using the chopped output of the lamp (Osram XBO high-pressure xenon lamp illuminating the electrode between 325 and 850 nm to avoid warming by NIR absorption and direct photolysis).

After checking and optimizing the system, the $NaClO_4$ aqueous solution was replaced by a $NaClO_4$ solution containing 10^{-4} M sodium salicylate (pH 3), and an oxygen flow of 20 mL/min was maintained into the solution. After obtaining a reproducible voltammogram in the dark, the electrode was biased at +0.6 V and illuminated again during a time *t*, when a sample of the solution was taken. The concentration of salicylate in the solution at time *t* was measured by the intensity of the band centered at 296 nm in the UV−vis spectrum. Once the experiment was completed, a new control voltammogram was run to confirm that the film remained intact during the overall process.

Results and Discussion

Sample Characterization. Mesoporous titania films samples produced using Pluronics F127 or Brij 58 templates were labeled TF-X or TB-X, respectively. "X" denotes the substrate: "S" for silicon, "F" for FTO, and "I" for ITO. Film deposition was followed by a stabilization posttreatment, to obtain robust samples with reproducible porosity and accessibility. Conductive glass or crystalline silicon were used as substrates. In all cases studied here, a mesostructure derived from a [110] oriented *Im3m* mesophase, uniaxially distorted in the *z*-axis, was obtained, as assessed by SAXS.[9,37] In the explored conditions, slow 1 °C min^{-1} heating ramps were used and samples were held for 2 h to temperatures between 250 and 450 °C. All films treated at $T < 350$ °C presented ordered mesostructures; no appreciable crystalline character was observed by WAXRD or TEM/selected-area electron diffraction (SAED). Films deposited on glass substrates retained highly organized porosity according to SAXS and TEM until 450 °C, as shown in Figure 1. No appreciable crystalline character was detected by WAXRD in any sample deposited on plain or conductive glass and treated until 450 °C, suggesting that the crystallinity is low, and the samples can be considered to be mostly amorphous. Anatase crystallites are detected by WAXRD in glass-supported samples after thermal treatments at $T > 500$ °C for times longer than 1 h. In those conditions, the mesostructure is practically collapsed after longer treatments. TEM images of the samples deposited on Si substrates and treated at temperatures higher than 350 °C show the emergence of denser walls, corresponding to anatase crystallites, as assessed by electron diffraction. Accordingly, anatase peaks are found in the WAXRD patterns of Si-supported samples, collected at fixed grazing incidence, in good agreement with previous work.[4,8−10] Crystallite size estimated by the Scherrer method ranges from 7 to 8.5 nm for Si-supported titania treated from 350 to 450 °C, in agreement with previous work. Coincident with the appearance of anatase, an increasing disorder in the mesostructure can be observed in the TEM pictures, which can be attributed to rearrangements in the pore walls, due to the confined growth of the nanocrystals.[8] SAXS patterns show a high degree of uniaxial contraction along temperature, as is normally observed in this kind of system.[7−9]

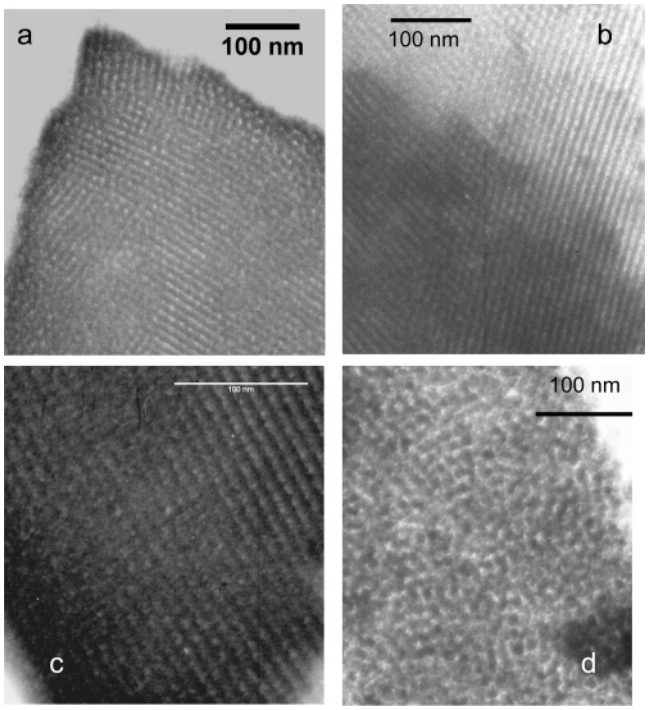

Figure 1. TEM images of F127-templated mesoporous titania films: (a) ITO-supported, treated at 300 °C; (b) ITO-supported, treated at 400 °C; (c) Si-supported, treated at 300 °C; (d) Si-supported, treated at 350 °C.

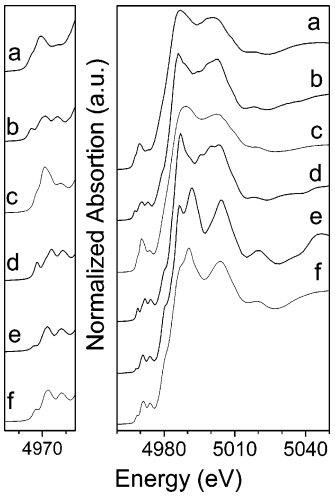

Figure 2. Pre-edge region (left) and complete XANES spectra (right) of mesoporous films F127/Si measured in air at room temperature and pretreated at 300 (a) and 400 °C (b). Spectra corresponding to amorphous-like TiO_2 (c), anatase (d), rutile (e), and brookite (f) are also included for comparison.

Characterization of Local Titania Structure by XANES. The XANES technique offers a detailed and quantitative picture of the local structure around Ti atoms. Figure 2 shows the Ti K XANES spectra for 150 nm thick TiO_2 mesoporous thin film samples deposited on Si (TF-S), treated at 300 and 400 °C and measured at room temperature, and the XANES spectra for

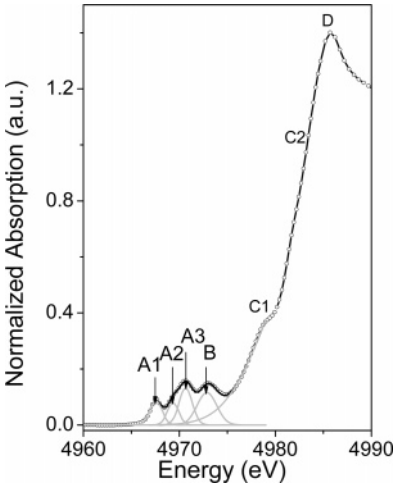

Figure 3. Pre-edge Ti K XANES region for anatase TiO_2. The experimental data are indicated with open circles. The different Gaussian fits of pre-peaks are labeled as A*i* ($i = 1-3$) and B. An additional peak at higher energy was also included just to account for the edge rising.

reference compounds: amorphous-like TiO_2, anatase, rutile, and brookite. A completely amorphous TiO_2 reference compound was obtained according to synthesis procedures described elsewhere.[38] From the comparison of spectra in the pre- and post-edge regions with the reference spectra, it can be concluded that the phase transition, when it occurs, leads to an anatase-like phase.

As shown in Figure 2 (left), the Ti K XANES pre-edge region is particularly suited to assess changes in the local Ti coordination associated with different postsynthesis treatments.[22,32] Titanium dioxide, particularly anatase, is a material extensively studied theoretically and experimentally by XANES.[21,31,39−45] The four pre-peaks in anatase phase (see Figure 3), labeled as A1, A2, A3, and B, correspond to transitions of the core electron to Ti 3d4p4s hybridized states. The A1 pre-peak is due to a t_{2g} bandlike state, whereas A2 and A3 are the results from e_g bandlike states. The t_{2g} and e_g states represent the components of the crystal field split Ti 3d atomic orbitals (AOs) which are shifted relative to each other in energy as a result of the octahedral oxygen surrounding of titanium.[46,47] The pre-peak A1 feature mainly originates from the first shell of four Ti neighbors at 3.04 Å, whereas the intensity of pre-peaks A2 and A3 is assigned to the transitions due to the second set of Ti neighbors at 3.78 Å. The Ti 3d AOs influence each other via hybridization with the oxygen orbital located in between. Transition B has a predominantly Ti 4p character hybridized with the Ti 4s and/or O 2p orbitals.[29] Pre-peaks C1 and C2 represent transitions of the core electron toward O 2p states that are hybridized with Ti 4p states, and D can be attributed to higher lying p AOs.[48]

Figure 4 shows the Ti K XANES pre-edge region for 150 nm thick TF samples after thermal treatment in still air and amorphous-like TiO_2 and anatase TiO_2 spectra for comparison (spectra 1 and 7, respectively). Samples deposited on ITO (TF-I, Figure 4a) present very slight changes in the spectrum, and the samples can be considered essentially amorphous after thermal treatment. The same phenomenon is observed on glass and FTO substrates, for TB and TF samples. On the other hand, Si-supported films show a sharp change in the peak features, which can be attributed to an amorphous to anatase transition, between the treatments at 300−350 °C. Essentially the same results are observed in nonmesoporous thin films prepared using

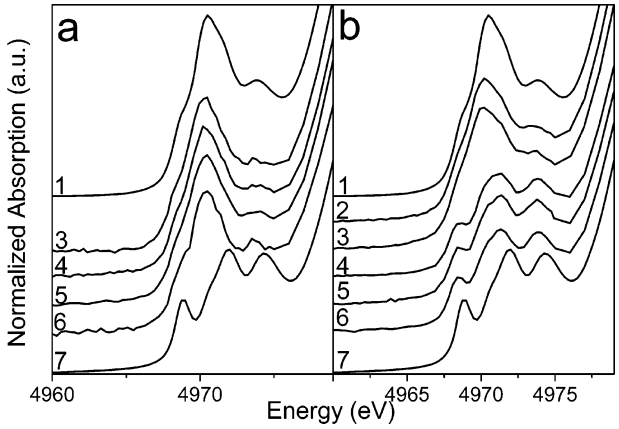

Figure 4. Ti K XANES raw data spectra of mesoporous thin films on ITO (a) and Si (b) substrates. Samples were treated at 250, 300, 350, 400, and 450 °C in air (labels 2, 3, 4, 5, and 6, respectively). Spectra labeled as 1 and 7 correspond to amorphous-like TiO_2 and crystalline anatase TiO_2, respectively.

the same deposition and treatment methods and template-free precursor solutions (see Supporting Information).

High-energy resolution allows distinguishing four peaks[48,26,49] at the Ti K-pre-edge region for anatase (A1, A2, A3, and B, A2 appears as a shoulder at the low-energy side of A3, see Figure 3). Thus, the qualitative information readily visible from the spectra in Figure 4 can be quantitatively established by adjusting the positions and areas of these four peaks.[31,32] The pre-edge region was fitted to four Gaussian curves A1, A2, A3, and B plus an extra peak C that accounts for the edge rising (see Figure 3).

Previous works reported that, as the TiO_2 anatase particle size decreases, the contribution of the peaks at the pre-edge region increases (peaks A2 and A3 in Figure 3).[21,49,50] This was interpreted as due to the large fraction of Ti atoms at the TiO_2 nanoparticle surface, indicating an increasing distortion from the octahedral TiO_6 unit. Conversely to Ti in a crystalline anatase environment, a distorted[20] or defective[33] Ti environment is expected in TiO_2 with poor crystallinity. Thus, the higher pre-peak intensity because of the higher orbital mixing between Ti and O (as was previously described in this section at the beginning) and/or the lower local coordination (pentacoordinated Ti respect to six-fold Ti in crystalline anatase) in Ti K XANES spectrum is representative of the low crystalline order with respect to the existing order in the crystalline anatase one.[38] Then, we propose the measurement of the relative amount of Ti with the same local symmetry defined by the six oxygen near neighbors as in crystalline TiO_2 anatase by the measurement of the "local anatase character". Thus this local character can be obtained by the fitting of the relative intensity of the middle peaks A2 and A3, with respect to the area of the pre-edge region at the Ti K-XANES spectra of the samples. A parameter, *L*, can be conveniently defined as the sum of A2 and A3 peak intensities divided by the total peak area A_T, where A_T is the sum of A1, A2, A3, and B peaks from the crystalline anatase used as standard: $L = (A2 + A3)/A_T$. In this way, *L* is the numerical weight, through the pre-peak intensity measurements, of Ti in defective, less coordinated Ti environments than in crystalline anatase; it indicates the degree of local resemblance of Ti in the samples with respect to Ti in crystalline anatase at the first environment of Ti atoms. The *L* value can be calculated for crystalline anatase and amorphous TiO_2, defining in this way the reference values for the corresponding compounds (see dotted horizontal lines in Figure 5) to have a direct and

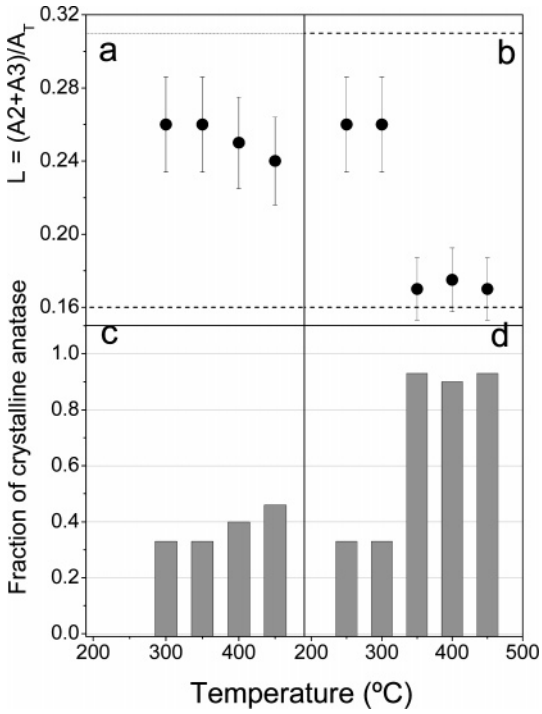

Figure 5. (top) *L* values for 150 nm thick TF samples supported on ITO (a) and Si (b). The upper horizontal dashed line corresponds to the *L* value for amorphous-like TiO_2, and the lower one corresponds to that obtained for crystalline reference anatase TiO_2. (bottom) Fraction of crystalline anatase obtained from *L* parameter for samples supported on ITO (with relative errors lower than 2%) and Si (with relative errors lower than 10%) substrates are shown in (c) and (d), respectively.

quantitative comparison between the Ti environment in the samples and in those reference compounds.

The determination of the *L* values for amorphous and crystalline anatase titania and the interpolation of a linear relationship for this parameter in the samples permit assessment of the degree of Ti in an anatase crystalline environment. Reference samples related to two extreme reference compounds were used. The 100% amorphous TiO_2 standard was obtained following the procedures indicated by Fernandez-García et al.;[26] a crystalline anatase TiO_2 reference compound was taken as a 100% crystallinity reference. It is possible then to calibrate a crystalline-anatase-like local environment fraction x_{An}, by simple interpolation of the characteristic *L* parameter value obtained for these standards, assuming linear behavior of the absorption in the pre-edge region. The degree of Ti with local environment as in crystalline anatase, x_{An}, was thus determined for each sample, by using the adjusted linear relationship between *L* and x_{An}: $L = 0.31 - 0.15x_{An}$.

The quantitative XANES analysis presented here permits assignment of the proportion of Ti in an anatase-type environment to low-temperature-treated titania samples that are classified as amorphous by routine XRD. It is interesting to note that the chloride synthesis route followed in this work seems to lead to samples with a small albeit noticeable crystalline character at 200−250 °C, for films deposited on all substrates. This behavior might be related to the high chloride contents of the precursor solutions, and in the initial stages of film treatment. It has been reported that titania nanoclusters (i.e., presenting local order) are the actual precursors of the inorganic walls.[9] The presence of chloride during consolidation treatments at moderate temperatures might help rearrangement of these initial titania nanobuilding blocks into ordered structures, which can resemble local crystalline order. Concentrated chloride has been held responsible for the formation of crystalline titania by Ostwald ripening of nanoparticles.[19]

Figure 5 shows the *L* values for 150 nm thick TF samples supported on ITO and Si, and the corresponding fraction of crystalline anatase TiO_2 on these films. The amorphous to anatase transition is deeply affected by the substrate. A well-defined transition is observed between the 300 and 350 °C treatments for the Si-supported films. The *L* values of the glass-supported samples are closer to the values expected for amorphous titania, and a slow increase of the crystalline character upon thermal treatment can be observed. This evolution is indeed incomplete in the conditions explored. The evolution to anatase seems to be also dependent on film thickness. Thicker mesoporous TF and TB films (400 nm, see Supporting Information) exhibit the same trend observed in Figure 5. However, the evolution to anatase on Si-supported films takes place between 350 and 400 °C. The difference between these two cases can be attributed to preferential nucleation at the film interfaces; thicker films evolve to crystalline materials in a slower fashion. Experiments are in progress to shed light on this.

After thermal treatments, the crystalline fraction in glass-supported films never exceeds 50%. It is interesting to notice that all glass-supported systems have not presented crystalline character by XRD until thermal treatment at 500 °C for more than 60 min (Supporting Information). XANES seems to be more sensitive than XRD in order to determine small "anatase-like" clusters. On the other hand, for Si-supported samples treated at $T > 300$ °C, the crystalline character quickly reaches 90% (Figure 5c,d). It is evident from this and Figure 5a,b that the amorphous to anatase transition on silica is sharper than on any glass substrate. The slow growth of the titania crystallites for the TF-I samples can be attributed to the kinetic stabilization of an amorphous titania, due to migration of Na^+ and Si^{4+} cations to the film. This process can lead to the formation of glasslike domains between the anatase nuclei detected by XANES on the titania surface. This glasslike "shell" located around the nanocrystals prevents the transport and rearrangement of Ti(IV) cations into larger crystalline units.

Photocatalytic Activity. The substrate dependence on crystallization found here is extremely important for the design of photoactive substrate−film electrodes, whether in photocatalysis or in photovoltaic devices such as photoelectrochemical cells.[1a] It has been previously observed that titania films deposited on glass substrates present typically lower crystalline character and thus poorer yields for conversion of light.[51−54] This can be attributed to several factors: (a) an influence of the crystalline character of the substrate (epitaxy effect), (b) electron−hole recombination sites due to migration of substrate components to the thin film; (c) lack of crystalline character due to the migration of cations from the substrate to the film.

Photoelectrocatalysis, i.e., photocatalysis under bias, provides a reproducible method for testing the activity of films in the photodegradation of organic compounds.[34] This is due to the higher band bending produced at positive potentials that minimizes electron−hole recombination at the solid electrolyte interface.[55] In addition, the method allows a direct measurement of photocatalytic activity without extra manipulation of the films, in relatively short times, which ensures minimum changes of the surface by a coupled process, such as photocorrosion.

The photocatalytic performance under bias of the 150 nm thick TF films deposited onto Si or ITO is summarized in Figure 6, where the photodegradation of salicylate measured in situ is expressed as the ratio of the absorbance at 296 nm at time *t*

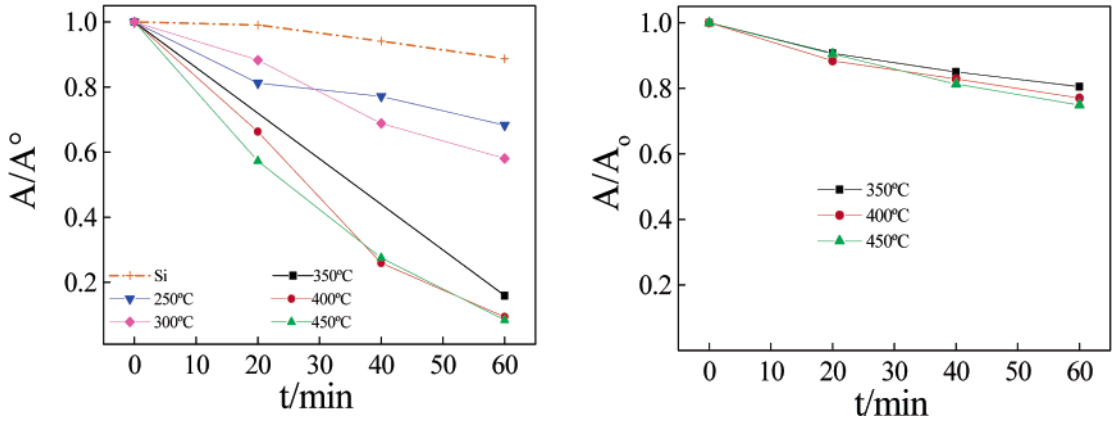

Figure 6. Photoelectrocatalytic performance of mesoporous titania thin films deposited on different substrates. Evolution of the relative absorbance of salycilic acid for TF samples supported on Si (a, left) and on ITO (b, right), and treated at different temperatures.

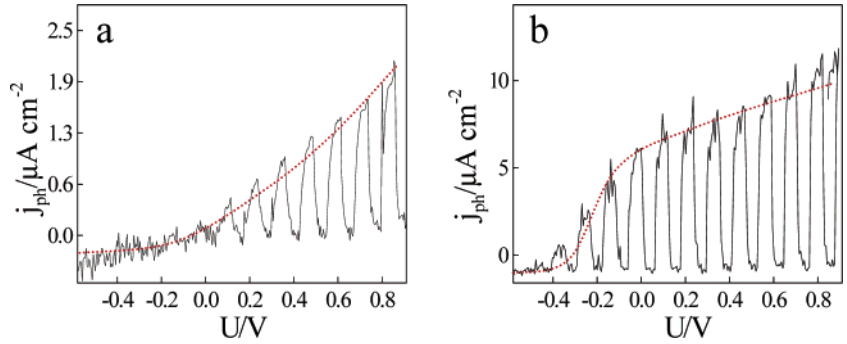

Figure 7. Photocurrent−voltage curves obtained for TF-S films treated at 300 (a) and 450 °C (b). The signal modulation observed is a consequence of dark−light cycles. The red envelope curves are a guide for the eye.

and initial conditions, i.e., $t = 0$ (A_t/A_0). Degradation of the organic molecule, defined as PD% = 100(1 − (A_t/A_0)), is low on the silicon or ITO substrates (PD% < 12% for Si, estimated as <5% for ITO). For silicon-supported films, a slight photodegradation (PD% < 40%) takes place in the films treated at T < 350 °C, where the anatase fraction is less than 30% (Figure 6a). A significant photocatalytic efficiency is observed (85−90% PD% within 60 min irradiation) when films present ca. 90% of anatase nanocrystallites.

Figure 6b shows the photocatalytic performance of glass-supported mesoporous titania films. In these samples, the degradation is notoriously smaller compared to the Si-supported films, in agreement with trends previously found with methylene blue over mesoporous titania films.[11,13b]

A comparison of the photocurrent voltage curves obtained by irradiating 150 nm thick TF-S films treated at 300 and 450 °C is shown in parts a and b, resepectively, of Figure 7. The shape of the photocurrent voltammogram obtained for the film treated at 300 °C is characteristic of an amorphous material;[56] the photovoltammogram of the high-temperature-treated film is attributable to a well-crystallized anatase electrode.[55,57] On the other hand, the maximum value of the photocurrent density is 4 times higher in the film treated at 450 °C than in the one treated at 300 °C. This difference agrees with the analysis of XANES spectra and WAXRD.

The photoelectrochemical response of the films treated to intermediate temperatures is governed by opposing effects, e.g., pore size increasing and surface area decreasing with increasing temperature.[11] The performance of the Si-supported films treated at T > 350 °C compares well with highly crystalline titania films produced by deposition of clear sols prepared from an alcoholic sol−gel route and treated at 400 °C.[58] This efficiency is due to the combination of the highly crystalline character and the accessible surface area available with mesoporous nanoanatase. Experiments are in progress to systematically study these issues, which will be presented in further work.

The preceding experiments demonstrate the importance of the substrate nature in anatase crystallization and photocatalysis performance. So far, two features can be identified: the effect of the substrate in the crystallization process and the effect of the substrate itself in the photocatalytic activity.

It is well-known that crystalline substrates favor the crystallization of deposited thin films upon thermal treatment. Fast anatase crystallization has been observed in mesoporous titania films deposited on silicon (111), platinum, or quartz substrates, in very good agreement with our work. Although no specific epitaxial effects have been reported, a monocrystalline substrate seems to lead to larger anatase crystallites than a polycrystalline one; this was attributed to an easier heterogeneous nucleation of nanoanatase on a crystalline surface.[53] It is interesting to remark that the reported studies about production of crystalline mesoporous titania films from molecular precursors mostly refer to Si-deposited samples.[8,9,11] This is also true for the first studies dealing with the crystallization mechanisms, where a discrepancy can be found in the stages of the nucleation−growth process; however, a fast and efficient crystallization process was always found and accurately followed by XRD.[17,18] On the other hand, many works report the correlation between diffusion of Na^+ cations from the glass substrate to the film, low titania crystallinity, and poor photocatalytic performance.[59] This process seems to be responsible for the lack of crystalline character of the glass-supported films, and the resulting low photocatalytic activity. The presence of other cations stabilizes the amorphous titania framework at the interface with the substrate, hindering the growth of anatase nuclei. This effect can in principle be avoided by treating the glass substrate prior to thin film

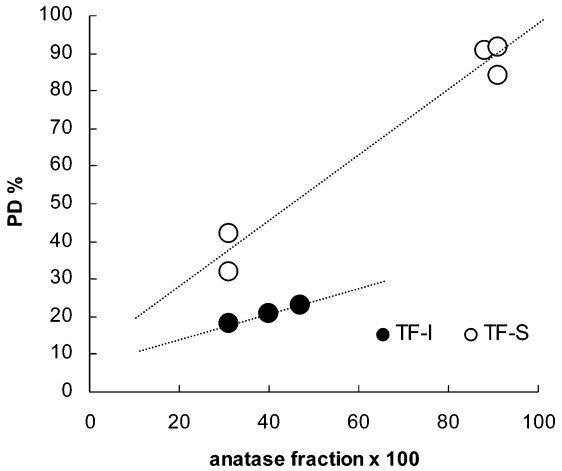

Figure 8. Correlation between the salicylate photodegradation (PD%) and the anatase fraction determined from XANES for 150 nm thick F127-templated titania thin films, deposited onto Si (○) or ITO (●) substrates. Dotted lines are a guide for the eye.

deposition. An acid treatment permits exchange of the surface sodium with protons, facilitating the production of nanocrystalline dense titania films;[51] deposition of a sol−gel silica dense thin film creates a barrier layer, which can favor anatase crystallization.[54,59] These aspects should be taken into account in order to fabricate transparent mesoporous nanocrystalline titania-based devices, supported on inexpensive substrates.

Apart from the correlation of crystal character versus photocatalysis observed, it seems that the role of the substrate can also be relevant in the catalytic process. Figure 8 shows a plot of PD% versus the anatase contents determined by XANES for TF samples. TF-S films present an appreciable photocatalytic activity (PD% on the order of 20−38%) below the massive conversion to anatase. By contrast, TF-I mesoporous films with an equal or higher anatase fraction than analogous TF-S systems present a significantly lower photocatalytic effect. In addition, the slope of the photocatalytic performance vs crystalline character is considerably smaller for TF-I samples than for the corresponding TF-S films. These facts point to an intervention of the substrate. Several hypotheses can be developed: (a) One is a difference in the substrate−film junction, which can influence the interfacial accumulation of charge carriers, hence modifying the transfer processes.[60] (b) Another is the role of the mobile cations cited above in the case of the glass substrates. Aside from hindering crystallization, migrating Si^{4+} and Na^{+} could partially form a glasslike layer on the titania surface, occluding reactive sites and therefore poisoning the catalyst. (c) These cations can behave as recombination centers,[61] therefore reducing the catalytic power of the titania surface.

Conclusion

We have synthesized mesoporous titania thin films with accessible porosity and nanocrystalline walls on conductive glass and silicon substrates. Ti K-edge XANES was used to assess Ti local coordination, and to quantify the fraction of Ti in anatase TiO_2 crystalline environment. This spectroscopic technique presents unique characteristics to characterize the local Ti symmetry and to study the crystal structure. Analysis of the pre-edge region permitted accurate quantification of the degree of crystalline nature of the inorganic walls upon thermal treatment, in a more sensitive way than what is performed by XRD. Small anatase-like domains are found in these films, at temperatures as low as 200 °C. This initial anatase content is a consequence of the synthesis route. Under the presented synthesis conditions, nucleation should not be an obstacle for crystallization, and growth should be the limiting step. The substrate has a marked effect in film crystallization upon thermal treatment: significant anatase formation takes place at temperatures 100−150 °C lower for films deposited on crystalline Si, compared to those made on conductive glass. This can be explained on the basis of migration of highly mobile cations from the glass substrate to the mesoporous film: an amorphous Na^{+}-containing titania phase is formed, which prevents growth of anatase nanocrystals. These amorphous domains might also occlude titania surface active sites. Both effects lead to a poor performance of the mesoporous titania deposited on conductive glass substrates. Excellent photocatalytic properties are found in well-crystallized mesoporous titania deposited onto conductive silicon. The combination of a powerful spectroscopic technique with structural analysis and photocatalytic behavior presented here leads to a better understanding of the processes needed to obtain porous robust photovoltaic or photocatalytic devices based on robust high-surface-area nanocrystalline oxides.

Acknowledgment. This work was funded by CONICET (PIP No. 6075, PIP No. 5191), ANPCyT (PAE 2004 Networks RENAMSI No. 22771, and MaN No. 22708, Research Grants PICT 06-12057, PICT 06-12345, PICT 06-17492, PICT 06-10621), UBACYT (X-093), Fundación Antorchas (14056-18), and Gabbos (GXNG-017). Synchrotron measurements were possible thanks to funding from LNLS, Campinas, Brazil: 2D SAXS, line D11A-SAS No. 3453/04 and No. 4286/05; XAS measurements: line D04B-XAFS1-4642 and 5121. P.C.A. acknowledges a Ph.D. grant from CNEA/CONICET; L.A. acknowledges a Ph.D. grant from CONICET. G.J.A.A.S.-I., F.G.R., and S.A.B. are staff members of CONICET. M.E.C. and G.J.A.A.S.-I. are members of Gabbos. The authors are indebted to L. I. Pietrasanta and N. De Vincenzo (CMA-UBA) for the TEM measurements, to M. Tamasi and J. Durán (Unidad de Actividad Física, CNEA) for provision of conductive silicon substrates, and to M. Fernández-García and J. Rodriguez for fruitful discussions.

Supporting Information Available: Ti K XANES spectra for 400 nm thick mesoporous titania films. This material is available free of charge via the Internet at http://pubs.acs.org.

References and Notes

(1) (a) Grätzel, M. *Nature* **2001**, *414*, 338. (b) Hoffman, M. R.; Martin, S. T.; Choi, W.; Bahnemann, D. W. *Chem. Rev.* **1995**, *95*, 69.

(2) Soler-Illia, G. J. A. A.; Sanchez, C.; Lebeau, B.; Patarin, J. *Chem. Rev.* **2002**, *102*, 4093.

(3) Soler-Illia, G. J. A. A.; Crepaldi, E. L.; Grosso, D.; Sanchez, C. *Curr. Opin. Colloid Interface Sci.* **2003**, *8*, 109.

(4) Grosso, D.; Cagnol, F.; Soler-Illia, G. J. A. A.; Crepaldi, E. L.; Amenitsch, H.; Brunet-Bruneau, A.; Bourgeois, A.; Sanchez, C. *Adv. Funct. Mater.* **2004**, *14*, 309.

(5) Soler-Illia, G. J. A. A.; Innocenzi, P. *Chem.—Eur. J.* **2006**, *12*, 4478.

(6) Alberius, P. C. A.; Frindell, K. L.; Hayward, R. C.; Kramer, E. J.; Stucky, G. D.; Chmelka, B. F. *Chem. Mater.* **2002**, *14*, 3284.

(7) Grosso, D.; Soler-Illia, G. J. A. A.; Babonneau, F.; Sanchez, C.; Albouy, P.-A.; Brunet-Bruneau, A.; Balkenende, A. R. *Adv. Mater.* **2001**, *13*, 14.

(8) (a) Crepaldi, E. L.; Soler-Illia, G. J. A. A.; Grosso, D.; Sanchez, C. *New J. Chem.* **2003**, *27*, 9. (b) Grosso, D.; Soler-Illia, G. J. A. A.; Crepaldi, E. L.; Cagnol, F.; Sinturel, C.; Bourgeois, A.; Brunet-Bruneau, A.; Amenitsch, H.; Albouy, P. A.; Sanchez, C. *Chem. Mater.* **2003**, *15*, 4562.

(9) Crepaldi, E. L.; Soler-Illia, G. J. A. A.; Grosso, D.; Cagnol, F.; Ribot, F.; Sanchez, C. *J. Am. Chem. Soc.* **2003**, *125*, 9770.

(10) Bartl, M. H.; Boettcher, S. W.; Frindell, K. L.; Stucky, G. D. *Acc. Chem. Res.* **2005**, *38*, 263.

(11) Sakatani, Y.; Grosso, D.; Nicole, L.; Boissière, C.; Soler-Illia, G. J. A. A.; Sanchez, C. *J. Mater. Chem.* **2006**, *16*, 77.
(12) Tang, J.; Wu, Y.; McFarland, E. W.; Stucky, G. D. *Chem. Commun.* **2004**, 1670.
(13) (a) Hwang, Y. K.; Lee, K. C.; Kwon, Y.-U. *Chem. Commun.* **2001**, 1738. (b) Lee, U.-H.; Lee, H.; Wen, S.; Mho, S.-I.; Kwon, Y.-U. *Microporous Mesoporous Mater.* **2006**, *88*, 48.
(14) Coakley, K. M.; McGehee, M. D. *Appl. Phys. Lett.* **2003**, *83*, 3380.
(15) Zukalovà, M.; Zukal, A.; Kavan, L.; Nazeeruddin, M. K.; Liska, P.; Grätzel, M. *Nano Lett.* **2005**, *5*, 1789.
(16) Bosc, F.; Ayral, A.; Albouy, P.-A.; Datas, L.; Guizard, C. *Chem. Mater.* **2004**, *16*, 2208.
(17) Choi, S. Y.; Mamak, M.; Speakman, S.; Chopra, N.; Ozin, G. A. *Small* **2005**, *1*, 26.
(18) Kirsch, B. L.; Richman, E. K.; Riley, A. E.; Tolbert, S. H. *J. Phys. Chem. B* **2004**, *108*, 12698.
(19) Pottier, A.; Cassaignon, S.; Chanéac, C.; Villain, F.; Tronc, E.; Jolivet, J.-P. *J. Mater. Chem.* **2003**, *13*, 877.
(20) (a) Montagna, M.; Dusi, R. *Phys. Rev. B* **1995**, *52*, 10080. (b) Mattarelli, M.; Montagna, M.; Rossi, F.; Chiasera, A.; Ferrari, M. *Phys. Rev. B* **2006**, *74*, 153412.
(21) Brydson, R.; Sauer, H.; Engel, W.; Thomas, J. M.; Zeitler, E.; Kosugi, N.; Kuroda, H. *J. Phys.: Condens. Matter* **1989**, *1*, 797.
(22) Chen, L. X.; Rajh, T.; Wang, Z.; Thurnauer, M. C. *J. Phys. Chem. B* **1997**, *101*, 10688.
(23) Farges, F.; Brown, G. E., Jr.; Rerh, J. J. *Phys. Rev. B* **1997**, *56*, 1809.
(24) Ruiz-López, M. F.; Muñoz-Páez, A. *J. Phys.: Condens. Matter* **1991**, *3*, 8981.
(25) Grunes, L. A. *Phys. Rev. B* **1983**, *27*, 2111.
(26) Matsuo, S.; Sakaguchi, N.; Wakita, H. *Anal. Sci.* **2005**, *21*, 805.
(27) Romano, C.; et al. *Am. Mineral.* **2000**, *85*, 108.
(28) Angelomé, P. C.; Soler-Illia, G. J. A. A. *Chem. Mater.* **2005**, *17*, 322.
(29) Otal, E. H.; Angelomé, P. C.; Aldabe-Bilmes, S.; Soler-Illia, G. J. A. A. *Adv. Mater.* **2006**, *18*, 934.
(30) Durham, P. J. In *X-ray Absorption: Principles, Applications, Techniques of EXAFS, SEXAFS and XANES*; Koningsberger, D. C., Prins, R., Eds.; Wiley-Interscience: New York, 1988.
(31) Notestein, J. M.; Andrini, L. R.; Kalchenko, V. I.; Requejo, F. G.; Katz, A.; Iglesia, E. *J. Am. Chem. Soc.* **2007**, *129*, 1122.
(32) Stewart, S. J.; Fernández-García, M.; Belver, C.; Mun, S. B.; Requejo, F. G. *J. Phys. Chem. B* **2006**, *110*, 16482.
(33) Ressler, T. *J. Synchrotron Radiat.* **1998**, *5*, 118.
(34) Calvo, M. E.; Candal, R. J.; Bilmes, S. A. *Catal. Today* **2002**, *76*, 133.
(35) (a) Regazzoni, A. E.; Mandelbaum, P.; Matsuyoshi, M.; Schiller, S.; Bilmes, S. A.; Blesa, M. A. *Langmuir* **1998**, *14*, 868. (b) Mandelbaum, P.; Aldabe Bilmes, S.; Regazzoni, E.; Blesa, M. A. *Solar Energy* **1999**, *65*, 75.
(36) (a) Vinodgopal, K.; Hotchandani, S.; Kamat, P. V. *J. Phys. Chem.* **1993**, *97*, 9040. (b) Kim, D. H.; Anderson, M. A. *Environ. Sci. Technol.* **1994**, *28*, 479.
(37) This orientation can also be described by an *Fmmm* orthorhombic mesostructure, as seen in: Urade, V. N.; Hillhouse, H. *J. Phys. Chem. B* **2005**, *109*, 10538.
(38) Fernández-García, M.; Wang, X.; Belver, C.; Hanson, J. C.; Rodríguez, J. A. *J. Phys. Chem. C* **2007**, *111*, 674.
(39) Ruiz-López, M. F.; Muñoz-Páez, A. *J. Phys.: Condens. Matter* **1991**, *3*, 8981.
(40) Wu, Z. Y.; Ouvrard, G.; Gressier, P.; Natoli, C. R. *Phys. Rev. B* **1997**, *55*, 10382.
(41) Grunes, L. A. *Phys. Rev. B* **1983**, *27*, 2111.
(42) Chen, L. X.; Rajh, T.; Jáger, W.; Nedeljkovic, J.; Thurnauer, M. C. *J. Synchotron Radiat.* **1999**, *6*, 445.
(43) Farges, F.; Brown, G. E., Jr.; Rehr, J. J. *Phys. Rev. B* **1997**, *56*, 1809.
(44) Luca, V.; Hanley, T. L.; Roberts, N. K.; Howe, R. F. *Chem. Mater.* **1999**, *11*, 2089.
(45) Fernández-García, M.; Martínez-Arias, A.; Hanson, J. C.; Rodríguez, J. A. *Chem. Rev.* **2004**, *104*, 4063.
(46) Orgel, L. *An Introduction to Transition-Metal Chemistry. Ligand-field theory*; Methuen & Co. Ltd.: London, 1964.
(47) Cotton, F. A. *Chemical Applications of Group Theory*; John Wiley and Sons Inc.: New York, London, Sydney, 1967.
(48) Brydson, R.; Sauer, H.; Engel, W.; Thomas, J. M.; Zeitler, E.; Kosugi, N.; Kuroda, H. *J. Phys.: Condens. Matter* **1989**, *1*, 797.
(49) Luca, V.; Djajanti, S.; Howe, R. F. *J. Phys. Chem. B* **1998**, *102*, 10650.
(50) Chen, L. X.; Rajh, T.; Jäger, W.; Nedeljkovic, J.; Thurnauer, M. C. *J. Synchroton Radiat.* **1999**, *6*, 445.
(51) Paz, Y.; Heller, A. *J. Mater. Res.* **1997**, *12*, 2759.
(52) Yu, J. C.; Yu, J.; Zhao, J. *Appl. Catal. B: Environ.* **2002**, *36*, 31.
(53) Zhang, Y.; Lin, J.; Wang, J. *Chem. Mater.* **2006**, *18*, 2917.
(54) Štangar, U. L.; Černigoj, U.; Trebsě, P.; Maver, K.; Gross, S. *Monatsh. Chem.* **2006**, *137*, 647.
(55) Flinkea, H. O. *Semiconductor Electrodes*; Elsevier: New York, 1988.
(56) Wilson, R. H. *J. Appl. Phys.* **1977**, *48*, 4292.
(57) (a) Tafalla, D.; Pujadas, M.; Salvador, P. *Surf. Sci.* **1989**, *215*, 190. (b) Tafalla, D.; Salvador, P. J. *Electroanal. Chem.* **1989**, *270*, 285.
(58) Yoldas, B. E. *J. Mater. Sci.* **1986**, *21*, 1087.
(59) Nam, H.-J.; Amemiya, T.; Murabayashi, M.; Itoh, K. *J. Phys. Chem. B* **2004**, *108*, 8254.
(60) Cao, Y.; Zhang, X.; Yang, W.; Du, H.; Bai, Y.; Li, T.; Yao, J. *Chem. Mater.* **2000**, *12*, 3445.
(61) Yu, H.; Yu, J.; Cheng, B. *Catal. Commun.* **2006**, *7*, 1000.